ELSEVIER

Journal of Structural Geology 27 (2005) 999–1010

JOURNAL OF STRUCTURAL GEOLOGY

www.elsevier.com/locate/jsg

Reverse and normal drag along a fault

Bernhard Grasemann[a,*], Steve Martel[b], Cees Passchier[c]

[a]Department of Geological Sciences, University of Vienna, Althanstr. 14, 1090 Vienna, Austria
[b]Department of Geology & Geophysics, University of Hawaii, Honolulu, HI, USA
[c]Department of Geosciences, University of Mainz, Mainz, Germany

Received 6 August 2004
Available online 9 June 2005

Abstract

An analysis of the theoretical displacement field around a single dip-slip fault at depth reveals that normal and reverse fault drag develop by perturbation flow induced by fault slip. We analytically model the heterogeneous part of the instantaneous displacement field of an isolated two-dimensional mode II fault in an infinite, homogeneous elastic body in response to fault slip. Material on both sides of the fault is displaced and 'opposing circulation cells' arise on opposite sides of the fault, with displacement magnitudes increasing towards the center of the fault. Both normal and reverse drag can develop at the fault center depending on the angle between the markers and the fault; normal drag develops there for low angles (<30–$40°$) and reverse drag for higher angles. A comparison of the theoretical results with published models and natural examples reveals that the characteristics of normal and reverse fault drag are largely insensitive to the scale and rheology of the faulted rocks and that drag forces generated by frictional resistance need not be the primary cause of fault drag. Fault drag has some interesting geometric implications for normal and reverse fault terminology emphasizing the importance for discrimination of vertical separation and throw. Furthermore, our results lead us to propose an alternative model for the formation of rollover anticlines above normal faults.

Keywords: Fault drag; Listric fault; Rollover; Analytical modeling; Stress function

1. Introduction

Fault drag refers to the deflection of curved markers adjacent to a fault (e.g. Kearey, 1993). *Normal drag* (Fig. 1) refers to markers that are convex in the direction of slip and *reverse drag* to markers that are concave in the direction of slip (e.g. Hamblin, 1965). Normal drag is probably the more commonly recognized phenomenon. Several explanations have been proposed to explain reverse drag, such as pre-brittle failure followed by reversal of movement on the fault, elastic and isostatic rebound, diapirism, sagging, differential compaction, and topological irregularities represented by fault overlap zones. Recognizing that reverse drag is not an abnormal structure but a common feature associated with normal faults, Hamblin (1965) suggested a model in which normal slip along a listric fault results in the formation of a rollover anticline. This model has appealed to petroleum geologists because of the potential of the anticline to form a hydrocarbon trap (e.g. Tearpock and Bischke, 2003) and has been widely accepted in structural geology textbooks (e.g. Twiss and Moores, 1992). However, Barnett et al. (1987) suggested that reverse drag results from a local decrease in displacement in the fault-normal direction and warned that hanging wall rollover anticlines cannot be used to distinguish listric from planar normal faults. Furthermore, Reches and Eidelman (1995) have shown by means of numerical modeling that fault drag reflects non-uniform deformation near a fault and that reverse drag may also form above anti-listric faults. While Reches and Eidelman (1995) demonstrated that drag effects can change along a single fault from reverse at its center to normal at its termination, they concluded (a) that reverse drag is mainly associated with 'short' faults (of unspecified length), and (b) that there is no consistent rule-of-thumb for fault drag. Grasemann et al. (2003) investigated with a finite element model the deflection of markers around a fault of finite length in a linear viscous medium. They considered various far-field velocity boundary conditions and

* Corresponding author. Tel.: +43 1 4277 53472; fax: +43 1 4277 9534.
E-mail address: bernhard.grasemann@univie.ac.at (B. Grasemann).

0191-8141/$ - see front matter © 2005 Elsevier Ltd. All rights reserved.
doi:10.1016/j.jsg.2005.04.006

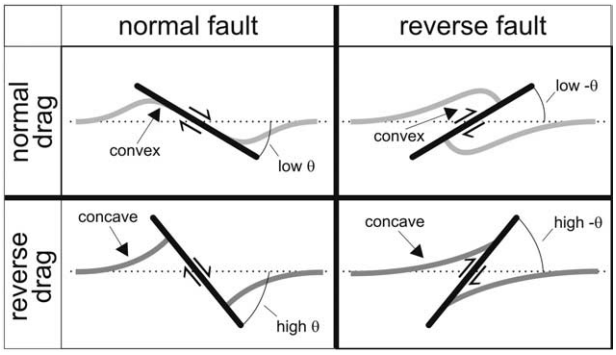

Fig. 1. Fault drag of a central marker along normal and reverse (thrust) faults. *Normal drag* refers to markers that are convex in the direction of slip and *reverse drag* to markers that are concave in the direction of slip. The angle θ is the acute angle measured from the fault to the undeformed central marker (anticlockwise angles are positive). The presented work demonstrates that low angles favor normal drag and high angles favor reverse drag.

compared the results with natural examples collectively called flanking structures (Passchier, 2001). Confirming the results of Reches and Eidelman (1995) that the drag of marker lines may change along a fault, Grasemann et al. (2003) showed that the drag of a central marker is only a function of the angle θ, the acute angle measured from the fault to the undeformed central marker (anticlockwise angles are positive). At low angles ($|\theta| < \sim 30°$) faults develop a normal drag but if the marker meets the fault at higher angles ($|\theta| > \sim 30°$) reverse drag develops (compare Fig. 1). Surprisingly, the model results suggest that the type of fault drag is independent of the kinematic vorticity number of the far-field deformation, but no further explanation why normal or reverse drag forms is given and therefore its origin is still unknown.

Our aim here is to demonstrate how normal and reverse drag can develop naturally because of heterogeneous deformation around a fault, in accord with previous suggestions (Barnett et al., 1987; Reches and Eidelman, 1995). We use predictions of standard linear elasticity theory to describe the displacement fields around a fault idealized as a mode II fracture. Note that we do not consider fault-inception folds (e.g. van der Pluijm and Marshak, 2004) that include all folds that developed during ductile deformation preceding faulting (e.g. fault folds, flexure faults). Furthermore, we do not model drag folds, which are folds that have formed by shear parallel to layering (Ramberg, 1963) but focus on folds that develop in response to single slip along a fault. However, we are aware that fault-inception folds, drag folds or pre-brittle failure followed by reversal of movement on the fault might result in similar geometric pictures discussed in this work. The major goal of this study is to explain the instantaneous development of fault drag along a single fault by investigating the heterogeneous part of the deformation field caused by fault slip. For the progressive developments of large strain, complex flanking structures, which may record rotation of faults and fault slip reversals, the readers are referred to the work of Exner et al. (2004) and references cited therein.

2. Conceptual model

When a fault slips, heterogeneous stress and displacement fields develop in the surrounding rock (Pollard and Segall, 1987). In order to understand the associated drag effects, we idealize a fault as a simple two-dimensional crack with plane strain sliding displacement (mode II) in an infinite elastic body. We also postulate that the driving stress $\Delta\sigma$, the difference between the shear traction on the fault before and after slip (Pollard and Segall, 1987), is uniform. The slip distribution on such a fault is elliptical, reaching a maximum at the center of the fault and dropping to zero at the fault tips (Rippon, 1985; Barnett et al., 1987; Pollard and Segall, 1987; Walsh and Watterson, 1989). A nearly elliptical slip pattern also is conceivable for a fault that is more than two fault lengths below the surface. Decidedly non-elliptical and asymmetric slip distributions can arise, however, for many reasons (Bürgmann et al., 1994), such as non-uniform driving stresses, irregular fault geometries, interactions with other faults, or intersections with a free surface (e.g. the earth's surface). Where the slip distribution is not elliptical, the complete displacement field will yield drag patterns different to those we describe here. We focus on certain first-order processes that lead to fault drag, and do not address important questions pertaining to the initiation and propagation of faults. Nor do we investigate the progressive development of fault drag along slip surfaces, which rotate or even may record a reversal of fault slip (Exner et al., 2004). We also ignore complex fault geometries. For modeling purposes we assume that all displacement except along the fault is accommodated by continuous deformation, although we are aware that on many natural faults a significant amount of discontinuous deformation is accommodated through secondary syn- and antithetic faults, secondary fracturing, or solution precipitation mechanisms (e.g. Walsh and Watterson, 1991; Martel and Boger, 1998).

The model here is based on linear elasticity theory and is idealized in terms of geometry, material properties and boundary conditions in order to highlight the first order influences of fault drag formation. The model captures the mechanics of an idealized single slip event or a series of events that do not include any stress relaxation. However, by setting Poisson's ratio to 0.5 and replacing the modulus of rigidity with the coefficient of viscosity and displacement magnitudes with velocity, the results can be directly translated to solutions for incompressible Newtonian viscous materials (Grasemann et al., 2003). Viscoelastic constitutive properties that would account for stress relaxation during accumulation of slip in a series of events are not considered. We emphasize, however, that the similar

geometries of fault drag in different lithologies and in a wide range of non- to high-grade metamorphic rocks (Passchier, 2001) suggest that certain basic characteristics of fault drag are largely scale independent. Existing theoretical treatments also reveal only a minor dependence on the rheology of the host rock (e.g. Barr and Houseman, 1992; Grasemann and Stüwe, 2001). In light of these findings, we contend that an elastic analysis should provide insight into fault drag.

Because we are interested in the instantaneous development of fault drag, which is caused by heterogeneous deformation induced by the fault slip, we ignore the homogeneous part of the deformation, which is a common procedure in analytical solutions (e.g. ignoring the second part of eq. 28.8 which is related to the remote stress in Pollard and Segall (1987)). In other words we focus on the heterogeneous deformation caused by the relative motion of a mode II crack ignoring any homogeneous background field. This displacement field is similar to the perturbation flow (e.g. Cobbold, 1975; Mancktelow, 1991), which has been recently used by Passchier et al. (2005) to classify natural structures. As a consequence the homogeneous background field and its orientation are immaterial for the origin (not the sense of slip, magnitude of drag, etc.) of fault drag, because homogeneous deformation cannot bend/fold/drag initially linear marker lines. For the further progressive development of fault drag the readers are referred to analogue and numerical models published elsewhere (Grasemann et al., 2003; Exner et al., 2004; Wiesmayr and Grasemann, 2005; Passchier et al., 2005).

The fault in our two-dimensional model extends along the x-axis from $x=-a$ to $x=a$. Displacements are confined to the x, y-plane and do not vary in the z-direction (i.e. we consider a plane strain case). Slip occurs if the ambient remote shear stress parallel to the fault differs from the shear traction on the fault, the difference of both is known as the driving stress $\Delta\sigma$. However, the uniform ambient stress field causes a homogeneous deformation field that does not contribute to fault drag (planar markers can be deformed but they remain planar). Therefore, we focus on the displacement field associated with slip on the fault, which results in a non-homogeneous deformation field responsible for the fault drag.

2.1. Stress functions for a mode II fault

We calculate the displacement field around a fault that has slipped using Westergaard stress functions (Westergaard, 1939; Tada et al., 2000). The interested reader can consult (Pollard and Segall, 1987; Bürgmann et al., 1994; Martel, 1997, 1999) for more detailed mathematical and physical aspects of these functions.

The displacement components u_x and u_y are found from two complex functions, and Z (Tada et al., 2000):

$$u_x = \frac{1}{2G}(2(1-\nu)\mathrm{Im}\,\bar{Z} + y\,\mathrm{Re}\,Z) \tag{1a}$$

$$u_y = \frac{1}{2G}(-(1-2\nu)\mathrm{Re}\,\bar{Z} - y\,\mathrm{Im}\,Z) \tag{1b}$$

where ν is Poisson's ratio, G is the modulus of rigidity (i.e. shear modulus), and

$$Z = \frac{\mathrm{d}\bar{Z}}{\mathrm{d}z} \tag{2}$$

The stress functions that yield the displacement field solely due to slip on a fault with a uniform driving stress are (Tada et al., 2000):

$$\bar{Z} = \Delta\sigma\left(\sqrt{z-a}\sqrt{z+a} - z\right) \tag{3a}$$

$$Z = \Delta\sigma\left(\frac{z}{\sqrt{z-a}\sqrt{z+a}} - 1\right) \tag{3b}$$

where $z=x+iy$. Note, that the term $\sqrt{z^2-a^2}$ is factored as $\sqrt{z-a}\sqrt{z+a}$ in order to yield correct values for the stress functions in all four quadrants of the complex plane (for a detailed discussion see Martel (1997)).

2.2. Displacement field near the center of a fault

The displacement field associated with fault slip is complex and heterogeneous. As a result, slip on a fault will cause an offset marker to be deformed as well. In order to describe this deformation as clearly as we can, we discuss the x- and y-components of the displacement field separately (Fig. 2). We pay particular attention to the effects on a marker that passes through the center of a fault; we henceforth call such a marker a central marker. As we will show, the deformation near the center of a fault is relatively uniform, so a marker does not need to pass precisely through the center of a fault to display the drag characteristics we discuss below.

First consider the displacement in the x-direction of a central marker perpendicular to the fault (Fig. 2a). The displacements along the marker are exclusively in the x-direction ($u_y=0$) and increase towards the fault:

$$u_x|_{x=0} = \frac{\Delta\sigma}{2G}a \times \left(\left[2(1-\nu)\sqrt{1+\left(\frac{y}{a}\right)^2}\right] - (3-2\nu)\left|\frac{y}{a}\right| + \frac{\left(\frac{y}{a}\right)^2}{\sqrt{1+\left(\frac{y}{a}\right)^2}}\right)\mathrm{sgn}(y) \tag{4a}$$

The radical terms can be expanded using the binomial theorem. Dropping terms of (y/a) higher than first order yields a simpler approximate expression:

$$u_x \approx \frac{\Delta\sigma}{2G}a\left([2(1-\nu)] - (3-2\nu)\left(\frac{y}{a}\right)\right) \tag{4b}$$

This matches eq. 8.59b of Pollard and Segall (1987) for the approximate value of u_x anywhere within roughly half a fault length from the fault center. Interestingly, Eq. (4b) is

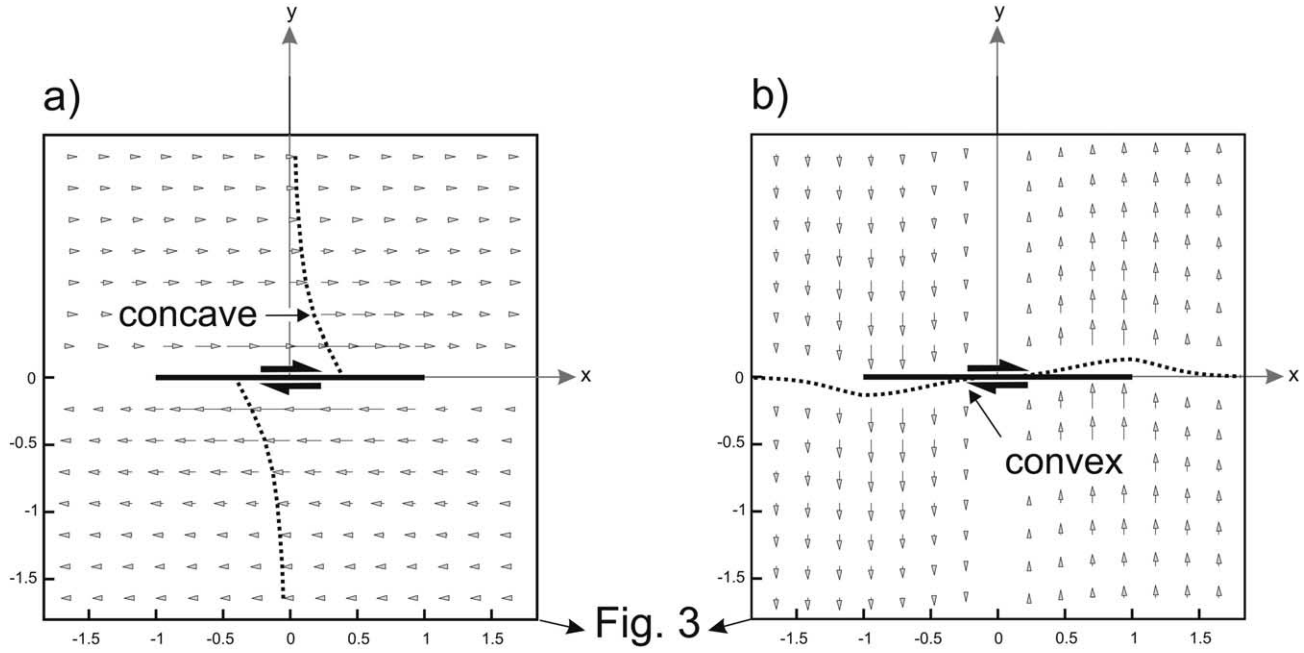

Fig. 2. Displacement fields in the (a) x-direction u_x and (b) y-direction u_y generated by dextral slip along a mode II fault from $-1<x<1$ at $y=0$. Poisson's ratio $\nu=0.3$ and the ratio of driving stress to the modulus of rigidity $\Delta\sigma/G=1/100$. In order to illustrate the heterogeneous deformation of the elastic solutions, displacements in the figures are exaggerated by a factor of 100 (Pollard and Segall, 1987). Marker lines (dotted line) perpendicular or at high angles to the fault will be primarily deformed by the *discontinuous* displacement field u_x into a concave shape in the shear direction and therefore record a reverse drag. Marker lines parallel or at low angles to the fault will be displaced predominantly by the *continuous* displacement field u_y into a convex shape recording a normal drag. The total displacement field composed of u_x and u_y are shown in Fig. 3.

not a function of x, reflecting the fact that u_x changes little with x near the center of the fault. The term in square brackets corresponds to the fault wall displacement at the center of the fault (i.e. half the maximum slip). The remainder of the expression reveals a nearly linear decay in u_x with distance from the fault; note that the terms containing Poisson's ratio are positive because υ is less than 0.5. The fault-parallel component of displacement causes a central marker perpendicular to the fault to be bent concave in the direction of slip: a reverse drag contribution develops. The same conclusion applies to fault-perpendicular markers near the fault center in light of Eq. (4b), as well as to originally planar markers of other orientations.

Now consider the displacement in the y-direction (Fig. 2b). We start by considering u_y along the plane of the fault, which has a simple, exact analytical form (Pollard and Segall, 1987):

$$u_y|_{y=0} = \Delta\sigma\frac{(1-2\nu)}{2G}x, \quad |x| \le a \tag{5a}$$

$$u_y|_{y=0} = \Delta\sigma\frac{(1-2\nu)}{2G}(x-\sqrt{x^2-a^2}), \quad |x| > a \tag{5b}$$

Figs. 2b and 3 show a counterclockwise rotation of the medium containing the fault for the 'apparent right-lateral' sense of slip depicted. For an opposite sense of slip, the rotation would be clockwise. Adjacent to the fault ($|x| \le a$, $y=0^{\pm}$) u_y is directly proportional to the distance from the center of the fault and the driving stress (see Eq. (5a)). This

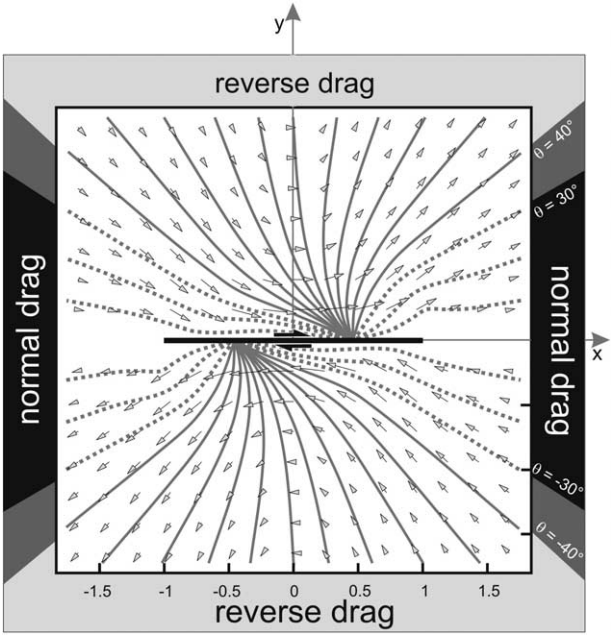

Fig. 3. Total displacement field near a dextral mode II fault and corresponding deformation of marker lines, initially passing through the origin at different angles. Marker lines meeting the fault at higher angles ($>\sim$30–40°) are dominated by the influence of u_x resulting in reverse fault drag. At lower angles ($<\sim$30–40°), however, where u_x is less significant, the deformation of the marker lines are mainly a function of u_y and therefore result in a normal fault drag (compare with Fig. 2).

means that the rock bordering the fault experiences a uniform rotation, with the amount of rotation scaling with the driving stress (Martel, 1999). Pollard and Segall (1987) show that Eq. (5a) is also the first-order solution for u_y anywhere within roughly half a fault length from the fault center. Analogous to the u_x field near the fault being nearly independent of x, the u_y field near the fault is nearly independent of y (compare Fig. 2a and b). The u_y field near the fault thus would cause a marker adjacent and parallel to the fault to be rotated but not bent. With increasing distance r from the fault center though, u_y (as well as u_x) decreases, eventually decaying as a/r. The rotation becomes negligible far from the fault. As a result, originally planar markers that are oblique to the fault are rotated more strongly near the fault center than they are far from the fault. This rotation change causes the marker to be bent (dragged) in a direction that is concave in the direction of slip. However, the fault-normal component of displacement causes a central marker oblique to the fault to be bent convex in the direction of slip: a normal drag contribution develops (this superposition of a normal drag on the reverse drag is discussed in more detail below, compare Fig. 7a and c). Although our focus is primarily on deformation of a marker near a fault, we show one example of how deformation along a long marker can be complicated (Fig. 2b). Consider a marker that intersects the fault at a shallow angle: at $x=a$, u_y attains its maximum amplitude (Eqs. (5a) and (5b)) and for $x>a$, u_y decreases monotonically towards zero. The marker is deformed in a complex wave-like shape with an inflexion point opposite the fault tip.

The total displacement field around a fault reflects a superposition of both the u_x and u_y components (Fig. 3). Whether a central marker displays normal or reverse drag will depend on the relative contributions of the displacement field to reverse drag and normal drag. Given the complexity of the displacement field around a fault, the sense of drag can vary with the orientation of a marker, where a marker intersects a fault, and the position along the marker. The difference between normal drag and normal drag superposed on reverse drag is outlined in more detail in the discussion section.

2.3. Drag of markers

The sense of drag depends on whether a marker becomes concave or convex in the direction of slip. We investigate now how the relative orientation of a fault and a marker affects the direction of marker curvature near a fault using the exact analytical expressions for the displacement field obtained from Eqs. (1a), (1b), (3a) and (3b). We calculate the curvature vector by fitting an osculating circle with radius R to three points on the deformed marker. The curvature κ, measured in diopters (m^{-1}), is given by:

$$\kappa = \frac{1}{R} \tag{6}$$

Close to the fault (i.e. within 1/10 of the fault half-length) our results show that normal drag (negative diopters) at the fault center arises for fault-marker angles $\theta < \sim 40°$, with reverse drag occurring for fault-marker angles $\theta > \sim 40°$ (dotted line in Fig. 4). However, in natural examples the drag very close to the fault might be difficult to recognize and it has therefore been suggested to investigate fault drag up to a distance of about half the fault-length (e.g. Barnett et al., 1987). If the central marker is evaluated at a larger distance to the fault (e.g. within 3/4 of the fault half-length) normal drag arises for fault-marker angles $\theta < \sim 30°$, with reverse drag occurring for fault-marker angles $\theta > \sim 30°$ (solid line in Fig. 4), which is consistent with results from finite element solutions of Grasemann et al. (2003).

Although our focus is on the fault center, we also investigate how the sense of drag can vary with position along a fault. The theoretical results here allow four classes of drag structures to be distinguished (Fig. 5). However, in order to understand the heterogeneous deformation induced by slip along a fault, we modeled the heterogeneous part of the deformation field without an imposed background strain. Therefore, the instantaneous structures in Fig. 5 cannot be directly compared with finite structures represented by the natural examples in Fig. 6. However, analogue and numerical models of finite deformation and the comparison of model results with natural examples (Grasemann et al., 2003; Exner et al., 2004; Wiesmayr and Grasemann, 2005) show that at low finite strain the geometries are very similar to the instantaneous structures presented in this study. For this reason, we think it is useful to refer to natural examples in the following discussion of our modeled structures, although we are aware that a direct comparison is inadequate.

2.3.1. Normal fault-normal drag

Large-scale examples are so-called 'low-angle' normal faults, which commonly reveal a normal drag (e.g. Wernicke, 1981). Other natural examples of this structure at smaller scale are shear bands (Berthé et al., 1979; White,

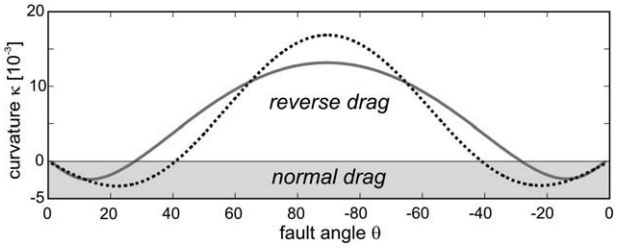

Fig. 4. Plot of fault angle θ versus the magnitude of the curvature κ of the central marker. Negative values for κ indicate a normal drag, whilst marker lines with a positive κ have a reverse drag. Close to the fault (1/10 of the fault half-length) normal drag arises for fault-marker angles $\theta < \sim 40°$, with reverse drag occurring for fault-marker angles $\theta > \sim 40°$ (dotted line). If the central marker is evaluated at a larger distance to the fault (3/4 of the fault half-length) normal drag arises for fault-marker angles $\theta < \sim 30°$, with reverse drag occurring for fault-marker angles $\theta > \sim 30°$ (solid line).

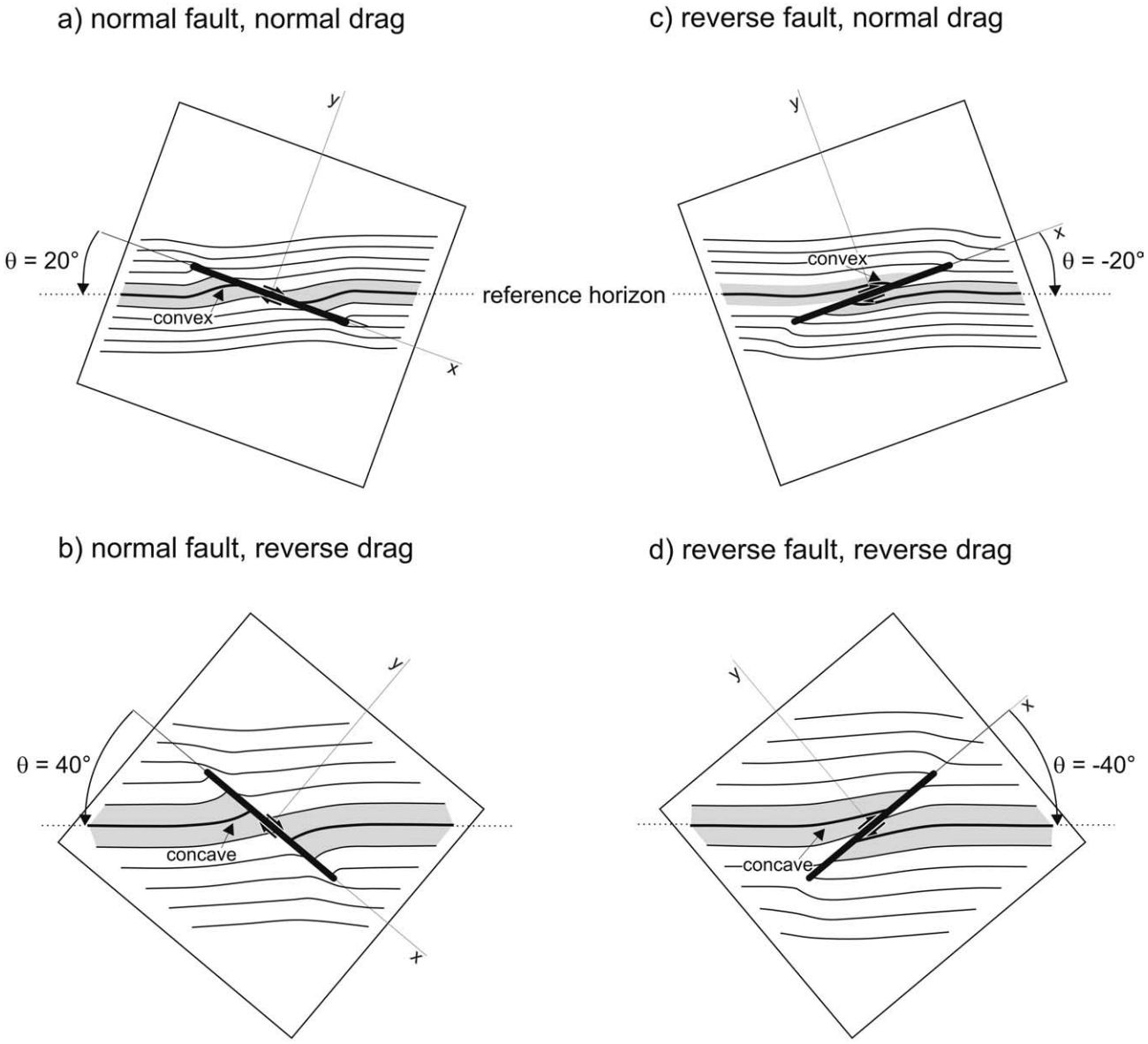

Fig. 5. Array of markers deflected by the displacement field (Eqs. (1a) and (1b)) generated by a fault of finite length (parameters and exaggeration see Fig. 2). In order to compare the model results with faults cutting through a horizontal layering or bedding, the coordinate system of Fig. 3 is rotated until the marker lines are parallel to a horizontal reference line. Dependent on the angle between the markers in the far field and the fault, four different structures can be distinguished: (a) normal fault–normal drag; (b) normal fault–reverse drag; (c) reverse fault–normal drag; (d) reverse fault–reverse drag.

1979), which are secondary synthetic slip surfaces. Statistically shear bands have low angles to the shear zone boundary (Passchier, 1984; Goscombe et al., 2004), but depending on the rheology, anisotropy and rotation during progressive deformation, shear bands may be also oriented at higher angles (Platt, 1984; Williams and Price, 1990; Stock, 1992). Typical natural examples of shear bands are illustrated in many publications. For example, Snoke et al. (1998) illustrate shear bands from many different rock types developed under a broad range of metamorphic conditions. Fig. 5a shows a central marker (in a heavy line) with normal drag from our model for $\theta = 20°$. Interestingly, normal drag also develops along the fault in the two quadrants where slip results in a decrease in the mean compressive stress, whereas reverse drag develops in the quadrants where the mean compressive stress increases. Although the orientation of the fault in the field example given in Fig. 6a is higher than in the instantaneous solution (Fig. 5a), the overall geometry of the fault drag of marker lines matches the geometry predicted by our model fairly well.

2.3.2. Normal fault-reverse drag

Hamblin (1965), who coined the term ‘reverse drag’, provided a superb example from the Hurricane Fault (Grand Canyon, Arizona) nearly four decades ago. Grasemann and Stüwe (2001), Passchier (2001) and Grasemann et al. (2003)

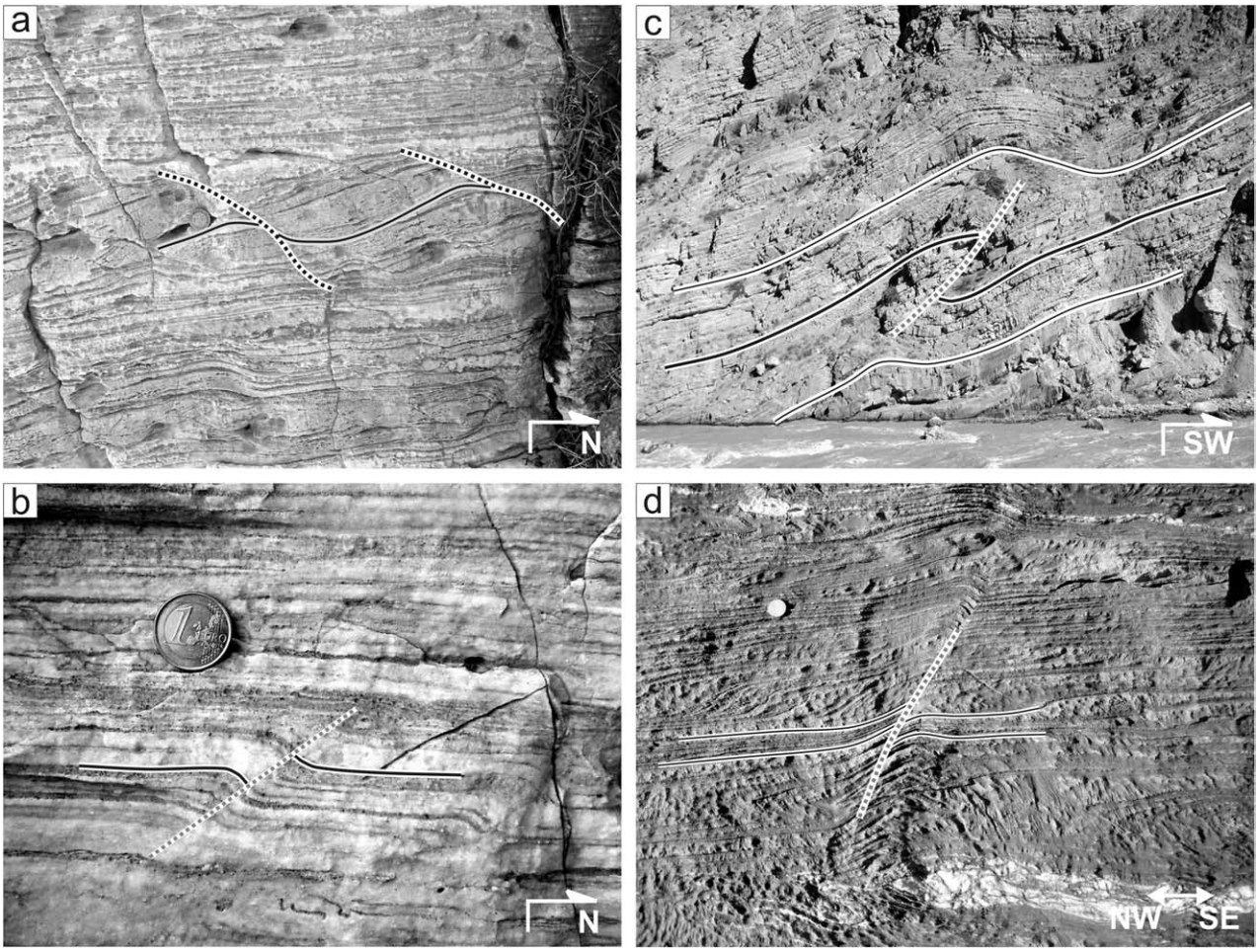

Fig. 6. Natural examples of structures modeled in Fig. 5. (a) Normal faults (shear band boudinage) in greenschist facies marbles mylonites showing a marked normal drag (N Naxos, Greece; N37°11′26.2″/E25°30′48.8″). (b) Normal fault with reverse drag from the same outcrop. (c) Reverse fault with normal drag in the Tethyan sediments of the fold and thrust belt in Spiti (Pin Valley, NW-Himalaya; N32°05′53.04″/E78°09′59.64″). Note the similarity of the structure with a fault propagation fold. (d) Reverse fault associated with reverse fault drag in marbles of the Goantagab Domain (Kaoko Belt, Namibia; S20°40″33.0″/E014°25″49.7″).

described other examples of reverse drag-along faults with extensional slip. Surprisingly few studies exist, however, that focus on the origin of reverse drag (e.g. Hamblin, 1965). Fig. 5b shows a central marker (in a heavy line) with reverse drag from our model for $\theta = 40°$. Note that the sense of drag changes along the model fault in Fig. 5b in a manner analogous to that of Fig. 5a. Our analytical results, represented in Fig. 5b, are consistent with the numerical results of Grasemann et al. (2003), and also similar to the field example of Fig. 6b. Reverse drag associated with regional normal faults is commonly referred to as a rollover anticline. Rollover anticlines typically are attributed to slip along listric normal faults, even though many reported examples of reverse drag do not occur along listric faults. Our model shows that reverse drag does not require curved fault geometry. We discuss this point further below.

2.3.3. Reverse fault-normal drag

Regional reverse faults with normal drag are widely recognized and are commonly attributed to folding that coincides with the upper tip of a thrust fault (e.g. Boyer, 1986; Suppe and Medwedeff, 1990). Passchier (2001) also presented natural examples of reverse faults with normal drag, terming the drag features ‘s-Type flanking folds’. An exceptional illustrative example from the Pin Valley in the NW-Himalayas is given in Fig. 6c. Most of the published examples are associated with a fault ramp that is connected to a flat detachment fault, and the footwall commonly is considered as undeformed (e.g. Jackson and McKenzie, 1983). We find that neither a flat detachment fault nor a rigid footwall is required for normal drag on a reverse fault. Footwall deformation along reverse faults generally has been interpreted as indicating folding preceding faulting during early development of break-thrust folds (Fischer et al., 1992). Nevertheless, McConnell et al. (1997) presented excellent natural examples of fault-related folds, where the hanging walls and footwalls are deformed, displacements decrease up- and down-dip from the centers of the faults,

and fault ramps do not join a flat-lying detachment. The kinematic model of McConnell et al. (1997) for folding yields geometric forms similar to our mechanical model (Fig. 5c). Note that normal drag of the central marker and at the leading edge of the reverse may be accompanied by reverse drag between the fault centers at the trailing tip. Our results thus should be distinguishable from folds considered to be break-thrust folds (Wiesmayr and Grasemann, 2005).

2.3.4. Reverse fault-reverse drag

Fig. 6d shows reverse drag along a reverse fault at a steep angle (~60°) to a mylonitic foliation. Although this structure has been predicted by mechanical finite element models (Grasemann et al., 2003), to our knowledge no natural example has been previously published. In the upper part of the picture above the tip of the fault a leading edge fold can be recognized. Towards the middle of the picture, the slip along the fault increases, revealing a pronounced reverse drag effect. This field example is consistent with our model results of Fig. 5d.

3. Discussion

3.1. Drag forces versus flow perturbation

Explanations of normal drag commonly have appealed to intuition. A typical suggestion invokes a reduction in the flow velocity of the wall rocks owing to frictional resistance along the fault. Therefore fault drag has been used to infer the sense of slip along faults (e.g. Hills, 1963; Billings, 1972; Twiss and Moores, 1992). This practice seems highly suspect to us, especially since the sense of drag can change along the same side of a fault. If drag was produced by frictional resistance to slip, then the amount of drag should increase with frictional resistance. However, mechanical models predict that if frictional resistance to slip increases, the slip on a fault decreases (Pollard and Segall, 1987) but also the drag decreases (Reches and Eidelman, 1995; Grasemann and Stüwe, 2001). Thus if frictional resistance accounted for drag, then the largest fault drag would be expected along faults with vanishing amounts of slip (i.e. where faults are absent; compare Fig. 6a, b and d). This conclusion is untenable. Finally, our investigation reveals that both normal and reverse drag can occur along a single fault (e.g. Figs. 5b and 6d; see also Mansfield and Cartwright, 2000), and that normal drag can be superposed on reverse drag (Figs. 5a and 6a). Frictional resistance cannot account for these observations either. We therefore, reject frictional resistance as a primary cause for fault drag.

3.2. Normal drag sensu stricto, vertical separation, and throw

Our analyses (Fig. 5a and c) and our observations (Fig. 6a and c) of faults show that 'normal drag' is in fact a superposition of a normal drag on the reverse drag associated with the fault-parallel displacement field. This has some interesting geometric implications for normal and thrust fault terminology. In our discussion here we follow the terminology of Tearpock and Bischke (2003), which reflects usage in the petroleum exploration community. We take vertical separation (*vs*) to be the vertical distance between very widely spaced points, which lie in a section perpendicular to the fault plane on opposing sides of a fault along a once continuous horizontal marker (Fig. 7). Throw

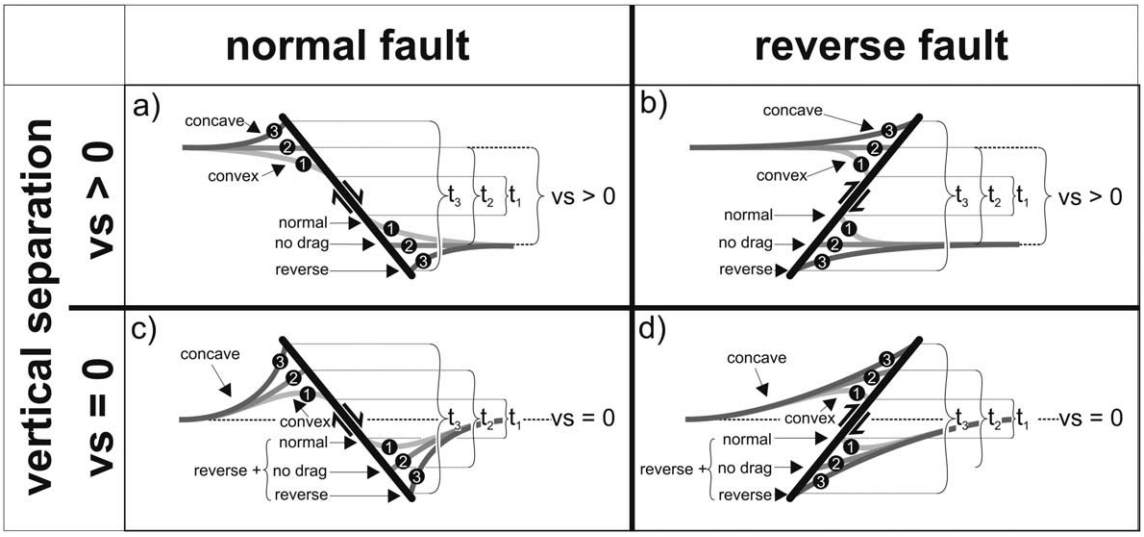

Fig. 7. Both vertical separation *vs* and throw *t* can be used to investigate possible fault drag geometries along normal ((a) and (c)) and reverse faults ((b) and (d)): if the throw is less than the vertical separation ($t_1 < vs$), then normal drag must exist (❶ in (a) and (b)). If the throw equals the vertical separation ($t_2 = vs$), then no net drag occurs (❷ in (a) and (b)). If throw exceeds the vertical separation ($t_3 > vs$) reverse drag must exist (❸ in (a) and (b)). If $vs = 0$, then the throw must exceed the vertical separation ($t_{1,2,3} > vs$ in (c) and (d)) and an offset horizontal marker must record reverse drag. Superposed on this reverse drag could be normal drag (❶), no drag (❷) or reverse drag (❸).

(t) is the vertical distance between piercing points on opposing walls of the fault. By these definitions, vertical separation is measured using points far from a fault, whereas throw relies on points that border a fault. As a result, vertical separation is independent of local displacements near a fault that produces fault drag, whereas throw depends strongly on fault drag. Pure normal drag or no drag is only possible geometrically if the vertical separation is greater than zero (Fig. 7).

Both vertical separation and throw can be used to investigate possible fault drag geometries of a marker through the center of a dip-slip fault (Fig. 7). Three cases are possible. First, the throw is less than the vertical separation ($t_1 < vs$), then normal drag must exist (Fig. 7a and b). Second, if the throw equals the vertical separation ($t_2 = vs$), then no net drag occurs. Third, if throw exceeds the vertical separation ($t_3 > vs$) reverse drag must exist. If no vertical separation occurs across a fault, then the throw must exceed the vertical separation ($t_{1,2,3} > vs$ in Fig. 7c and d). In such a case, an offset horizontal marker must record reverse drag. Superposed on this reverse drag could be normal drag (t_1), no drag (t_2) or reverse drag (t_3). A major result of this simple geometrical observation is that any fault with no vertical separation must have fault drag. Additionally, if no drag occurs across a fault, then vertical separation must occur. Because the established terminology is insufficient to describe complex fault drag geometries, Coelho et al. (2005) have recently suggested a new quantitative descriptive terminology using cubic Bézier curves.

3.3. Listric faults and rollover anticlines

The concept of a listric (based on the Greek word *listron* or shovel), concave-up normal fault was introduced by Suess (1909) as part of his description of curved faults in the coal mines of Saint-Eloi and Léon (northern France). They are now recognized in many places around the world (e.g. Shelton, 1984). Three features have been considered as characteristic of listric normal faults: a flat detachment surface, a rigid footwall, and hanging wall strata with a dip that increases toward a normal fault (i.e. rollover anticline or reverse drag; Shelton, 1984). Balanced cross-section analyses of listric faults are widely applied to investigate these features, to quantify regional extension, and in the exploration for hydrocarbons (e.g. Tearpock and Bischke, 2003). Rollover anticlines, for example, are one of the most important hydrocarbon traps (Tearpock and Bischke, 2003 and references cited therein). Since these methods also are used to assess the geometry of normal faults, which can seal subsurface fluid flow, they are important in defining the volume of a hydrocarbon reservoir (Hardman and Booth, 1991). The impact and widespread use of listric fault models prompt us to re-examine two of the commonly held perceptions about these faults.

We start with the assumption that a hanging wall rollover implies a listric fault geometry (e.g. Shelton, 1984 and references therein). This assumption seems highly precarious to us. First, although listric faults appear common, not all normal faults have listric geometries. For example, seismic reflection data commonly indicate normal fault traces that are not concave up in cross-sections (e.g. Jackson, 1987). Additionally, earthquake data provide little evidence for the notion that large-scale normal faults invariably flatten with depth. Second, reverse drag and rollover-like geometries occur at all scales and within a broad range of different homogeneous and heterogeneous rheologies (compare the presented and referenced examples in this work), including faults that have non-listric geometries. Third, in addition to our results, many mechanical models of planar faults (King et al., 1988; Gibson et al., 1989; Ma and Kusznir, 1993; Reches and Eidelman, 1995; Grasemann et al., 2003) show reverse drag. So listric fault geometries are not a prerequisite for reverse drag to develop. Our results show instead that reverse drag can be a consequence of heterogeneous perturbation deformation as a result of fault slip. Although other mechanisms before, during or after faulting could affect the development of reverse fault drag, we are in accord with Barnett et al. (1987) who suggested that the displacement field associated with slip is the primary cause for reverse drag (e.g. Fig. 5b).

The second perception that appears suspect to us is that the footwall of a normal fault is rigid. This assumption has no mechanical basis, and it certainly does not make sense in cases where rocks of similar lithology (or rheology) are juxtaposed by faulting (Kusznir et al., 1991). Indeed, geodetic measurements for single slip events, high-resolution three-dimensional seismic data sets, and detailed investigations of faults in outcrops commonly reveal reverse drag profiles in both the hanging wall and footwall (Kasahara, 1981; McConnell et al., 1997; Mansfield and Cartwright, 2000). A few reasons might contribute to the perception that fault footwalls are rigid.

The first is that displacements (and drag effects) in the footwall can be much less than those in the hanging wall. Such an association would be strong evidence for a stiffness difference for faults that are substantially deeper than their down-dip extent (i.e. faults that behave as though they were in an infinite body). Mechanical analyses of normal faults that intersect or interact with the earth's surface, however, reveal decidedly different slip profiles from faults far from the surface. Surface-breaching faults or near-surface faults tend to have a slip maximum at or near the surface rather than near the fault center; they offset markers in a manner somewhat similar to that in the lower half of Fig. 5b. Perhaps more significantly though, unlike faults in an infinite elastic body with no free surface, normal faults in an elastic half-space generate an asymmetric displacement field, with greater displacement (and more pronounced drag) in the hanging wall than in the footwall (Ma and Kusznir, 1993; Roberts and Yielding, 1994; Langley, 2000). The contrast in displacement could be mistaken for an

increase in rigidity in the footwall, when it actually reflects a difference in the 'effective thickness' of the units on the opposing sides of the fault. For a fault near the surface, the hanging wall is thin relative to the 'infinitely thick' footwall. Rigidity (i.e. the shear modulus) is an intrinsic property of a rock and does not depend on the geometry of a rock body. It should not be confused with 'flexural rigidity', the resistance to bending, which is highly dependent on the geometry of a body (Turcotte and Schubert, 2002).

A second reason that might contribute to the perception that fault footwalls are rigid is that reverse drag on either side of the fault may be associated with little of no drag on the opposing side, especially if structural levels above or below the central marker are observed (compare Figs. 4 and 5).

A third reason relates to the ease of preparing physical models with rigid footwalls (e.g. McClay et al., 1991) that yield hanging wall deformation akin to that in outcrops or inferred in seismic cross-sections. The similarity in results does not mean that the footwalls of faults in the earth are rigid though.

Listric fault models and the associated hanging wall rollover have been extensively applied by many workers to quantify regional extension, probably due to the ease with which hanging wall collapse may be restored using the vertical shear construction or one of its many derivatives (Yamada and McClay, 2003). However, because these techniques commonly are predicted on the assumption of a listric fault geometry (Tearpock and Bischke, 2003), they will necessarily predict a listric geometry even for faults that are planar. A simple example how a listric fault can be balanced from a modeled planar normal fault with reverse drag is given in Fig. 8.

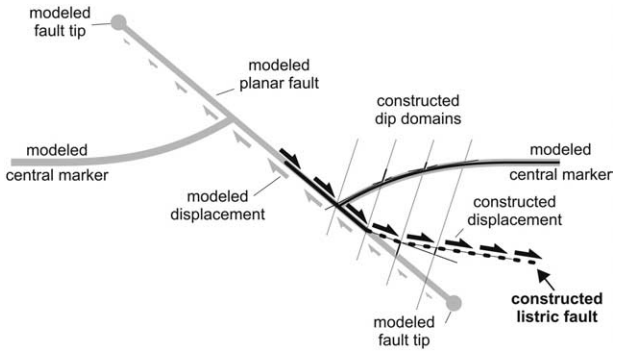

Fig. 8. Listric fault balanced from a modeled planar normal fault with variable displacement and reverse drag of the central marker line. Using the reverse drag of the central marker in the hanging wall and the dip of the fault at the intersection with the marker as input parameters, the graphical dip domain technique (Yamada and McClay, 2003) can be applied by incorrectly assuming that the reverse drag has been generated by constant slip along a listric fault. The dip of the domains has been obtained by determining the Coulomb collapse angle (72°) from the reverse drag shape (Tearpock and Bischke, 2003). The technique will necessarily result in a listric geometry, although the result is obviously wrong.

4. Conclusions

The presented analytical solutions of slip along mode II faults and the resulting fault drag are mechanically grounded predictable geometries, which match natural structures. Therefore, we conclude:

(1) Slip along a fault causes a heterogeneous displacement field, with increasing displacement magnitudes towards the fault. This heterogeneous displacement field will cause marker units to be deformed in a manner consistent with what has been called fault drag.
(2) Near the center of a fault, the sense of fault drag is mainly a function of the angle between the marker and the fault plane: low angles favor normal drag and high angles favor reverse drag.
(3) Normal and reverse drag can develop along the same side of a single fault.
(4) A comparison of model results, published models, and natural examples reveals that many key characteristics of normal and reverse fault drag are largely insensitive to the scale of a fault and the rheology of the host rock.
(4) Frictional resistance to slip along a fault cannot explain observations of fault drag, and is therefore not the primary cause of fault drag.
(5) Understanding the spatial geometry and development of fault drag is important for discrimination of vertical separation and throw of normal and thrust faults. Faults recording no vertical separation in the far field inherently have a reverse drag on which a normal drag can be superimposed.
(6) The concept of rollover anticlines forming above listric extensional faults may be alternatively explained by reverse fault drag. The reverse drag model may be a superior explanation for rollover anticlines, especially for normal faults that do not flatten into a subhorizontal detachment or are not listric at all.

Acknowledgements

We benefited from discussions with R. Scheichl, N. Mancktelow, Ulrike Exner, G. Wiesmayr, T. Kocher, H. Rice, E. Draganits and M. Edwards. K. Arnberger and M. Habermüller provided the picture of the reverse fault in the Pin Valley shown in Fig. 6c. The work was funded by the Austrian Science Foundation project number P-15668 and is SOEST contribution no. 6351. Critical reviews from Chris Talbot and Paul Williams and comments of the editor João Hippertt are gratefully acknowledged.

References

Barnett, J.A.M., Mortimer, J., Rippon, J.H., Walsh, J.J., Watterson, J., 1987.

Displacement geometry in the volume containing a single normal fault. The American Association of Petroleum Geologist Bulletin 71, 925–937.

Barr, T.D., Houseman, G.A., 1992. Distribution of deformation around a fault in a non-linear ductile medium. Geophysical Research Letters 19, 1145–1148.

Berthé, D., Choukroune, P., Jegouzo, P., 1979. Orthogneiss, mylonite and non coaxial deformation of granites: the example of the South Armorican shear zone. Journal of Structural Geology 1, 31–43.

Billings, M.P., 1972. Structural Geology. Prentice-Hall, Englewood Cliffs, NJ.

Boyer, S.E., 1986. Styles of folding within thrust sheets: examples from the Appalachians and Rocky Mountains of the USA and Canada. Journal of Structural Geology 8, 325–339.

Bürgmann, R., Pollard, D.D., Martel, S.J., 1994. Slip distributions on faults: effects of stress gradients, inelastic deformation, heterogeneous host-rock stiffness, and fault interaction. Journal of Structural Geology 16, 1675–1690.

Cobbold, P.R., 1975. Fold propagation in single embedded layers. Tectonophysics 27, 333–351.

Coelho, S., Passchier, C.W., Grasemann, B., 2005. Classification of fault drag. Journal of Structural Geology 27, 597–606.

Exner, U., Mancktelow, N.S., Grasemann, B., 2004. Progressive development of s-type flanking folds in simple shear. Journal of Structural Geology 26, 2191–2201.

Fischer, M.P., Woodward, N.B., Mitchell, M.M., 1992. The kinematics of break-thrust folds. Journal of Structural Geology 14, 451–460.

Gibson, H.D., Walsh, J.J., Watterson, J., 1989. Modelling of bed contours and cross-sections adjacent to planar normal faults. Journal of Structural Geology 11, 317–328.

Goscombe, B.D., Passchier, C.W., Hand, M., 2004. Boudinage classification: end-member boudin types and modified boudin structures. Journal of Structural Geology 26, 739–763.

Grasemann, B., Stüwe, K., 2001. The development of flanking folds during simple shear and their use as kinematic indicators. Journal of Structural Geology 23, 715–724.

Grasemann, B., Stüwe, K., Vannay, J.-C., 2003. Sense and non-sense of shear in flanking structures. Journal of Structural Geology 25, 19–34.

Hamblin, W.K., 1965. Origin of 'reverse drag' on the down-thrown side of normal faults. Geological Society of America Bulletin 76, 1145–1164.

Hardman, R.F.P., Booth, J.E., 1991. The significance of normal faults in the exploration and production of North Sea hydrocarbons. In: Roberts, A.M., Yielding, G., Freeman, B. (Eds.), The Geometry of Normal Faults Geological Society Special Publication, vol. 56, pp. 1–16.

Hills, E.S., 1963. Elements of Structural Geology. Methuen and Co, London.

Jackson, J.A., 1987. Active normal faulting and crustal extension. In: Coward, M.P., Dewey, J.F., Hancock, P.L. (Eds.), Continental Extensional Tectonics Geological Society Special Publication, vol. 28, pp. 3–17.

Jackson, J., McKenzie, D., 1983. The geometrical evolution of normal fault systems. Journal of Structural Geology 5, 471–482.

Kasahara, K., 1981. Earthquake Mechanics. Cambridge University Press, Cambridge.

Kearey, P., 1993. The Encyclopedia of the Solid Earth Sciences. Blackwell Science, Oxford.

King, G.C.P., Stein, R., Rundle, J., 1988. The growth of geological structures by repeated earthquakes, 1: conceptual framework. Journal of Geophysical Research 93, 13307–13318.

Kusznir, N.J., Marsden, G., Egan, S.S., 1991. A flexural-cantilever simple-shear/pure-shear model of continental lithosphere extension: applications to the Jeanne d' Arc Basin, Grand Banks and Viking Graben, North Sea. In: Roberstss, A.M., Yielding, G., Freeman, B. (Eds.), The Geometry of Normal Faults Geological Society Special Publication, vol. 56, pp. 41–60.

Langley, J.S., 2000. Processes of normal faulting and surface deformation along the Koae fault system, Hawaii. Unpublished MS thesis, University of Hawaii.

Ma, X.Q., Kusznir, N.J., 1993. Modelling of near-field subsurface displacements for generalized faults and fault arrays. Journal of Structural Geology 15, 1471–1484.

Mancktelow, N.S., 1991. The analysis of progressive deformation from an inscribed grid. Journal of Structural Geology 13, 859–864.

Mansfield, C.S., Cartwright, J.A., 2000. Stratal fold patterns adjacent to normal faults: observations from the Gulf of Mexico. In: Cosgrove, J.W., Ameen, M.S. (Eds.), Forced Folds and Fractures Geological Society Special Publication, vol. 169, pp. 115–128.

Martel, S.J., 1997. Effects of cohesive zones on small faults and implications for secondary fracturing and fault trace geometry. Journal of Structural Geology 19, 835–847.

Martel, S.J., 1999. Mechanical controls on fault geometry. Journal of Structural Geology 21, 585–596.

Martel, S.J., Boger, W., 1998. Geometry and mechanics of secondary fracturing around small three-dimensional faults in granitic rock. Journal of Geophysical Research 103, 21299–21314.

McClay, K.R., Waltham, D.A., Scott, A.D., Abousetta, A., 1991. Physical and seismic modelling of listric normal fault geometries. In: Roberstss, A.M., Yielding, G., Freeman, B. (Eds.), The Geometry of Normal Faults Geological Society Special Publication, vol. 56, pp. 231–240.

McConnell, D.A., Kattenhorn, S.A., Benner, L.M., 1997. Distribution of fault slip in outcrop-scale fault-related folds, Appalachian Mountains. Journal of Structural Geology 19, 257–267.

Passchier, C.W., 1984. The generation of ductile and brittle shear bands in a low angle mylonite zone. Journal of Structural Geology 6, 273–281.

Passchier, C.W., 2001. Flanking structures. Journal of Structural Geology 23, 951–962.

Passchier, C.W., Mancktelow, N., Grasemann, B., 2005. Flow perturbations: a tool to study and characterize heterogeneous deformation. Journal of Structural Geology. doi:10.1016/jsg.2005.01.016.

Platt, J.P., 1984. Secondary cleavages in ductile shear zones. Journal of Structural Geology 6, 439–442.

Pollard, D.D., Segall, P., 1987. Theoretical displacements and stresses near fractures in rocks. In: Atkinson, B.K. (Ed.), Fracture Mechanics of Rock. Academic Press, London, pp. 277–349.

Ramberg, H., 1963. Evolution of drag folds. Geological Magazine 100, 97–106.

Reches, Z., Eidelman, A., 1995. Drag along faults. Tectonophysics 247, 145–156.

Rippon, J.H., 1985. Contoured patterns of throw and hade of normal faults in the coal measures (Westphalian) of northeast Derbyshire. Proceedings of the Yorkshire Geological Society 45, 147–161.

Roberts, A.M., Yielding, G., 1994. Continental extensional tectonics. In: Hancock, P.L. (Ed.), Continental Deformation. Pergamon Press, Oxford, pp. 223–250.

Shelton, W., 1984. Listric normal faults: an illustrated summary. The American Association of Petroleum Geologist Bulletin 68, 801–815.

Snoke, A.W., Tullis, J., Todd, V.R., 1998. Fault-related Rocks. Princeton University Press, Princeton, NJ.

Stock, P., 1992. A strain model for antithetic fabric rotation in shear band structures. Journal of Structural Geology 14, 1267–1275.

Suess, E. 1909. Das Antlitz der Erde. Tempsky, F.; Freytag, G., Prag and Wien; Leipzig.

Suppe, J., Medwedeff, D.A., 1990. Geometry and kinematics of fault-propagation folding. Eclogae Geologicae Helvetiae 83, 409–454.

Tada, H., Paris, P.C., Irwin, G.R., 2000. The Stress Analysis of Cracks Handbook. The American Society of Mechanical Engineers, New York.

Tearpock, D.J., Bischke, R.E., 2003. Applied Subsurface Geological Mapping. Prentice Hall, New Jersey.

Turcotte, D.L., Schubert, G., 2002. Geodynamics. Cambridge University Press, Cambridge.

Twiss, R.J., Moores, E.M., 1992. Structural Geology. W.H. Freeman and Company, New York.

van der Pluijm, B., Marshak, S., 2004. Earth Structure—an Introduction to Structural Geology and Tectonics. WCM/McGraw-Hill, New York.

Walsh, J.J., Watterson, J., 1989. Displacement gradients on fault surfaces. Journal of Structural Geology 11, 307–316.

Walsh, J.J., Watterson, J., 1991. Geometric and kinematic coherence and scale effects in normal fault systems. In: Robersts, A.M., Yielding, G., Freeman, B. (Eds.), The Geometry of Normal Faults Geological Society Special Publication, vol. 56, pp. 193–206.

Wernicke, B., 1981. Low-angle normal faults in the Basin and Range Province-Nappe tectonics in an extending orogen. Nature 291, 645–648.

Westergaard, H.M., 1939. Bearing pressures and cracks. Journal of Applied Mechanics 66, 107–125.

White, S., 1979. Large strain deformation: report on a Tectonic Studies Group discussion meeting held at Imperial College, London on 14 November 1979. Journal of Structural Geology 1, 333–339.

Wiesmayr, G., Grasemann, B., 2005. Sense and non-sense of shear in flanking structures with layer-parallel shortening: implications for fault-related folds. Journal of Structural Geology 27, 249–264.

Williams, P.F., Price, G.P., 1990. Origin of kinkbands and shear-band cleavage in shear zones; an experimental study. Journal of Structural Geology 12, 145–164.

Yamada, Y., McClay, K., 2003. Application of geometric models to inverted listric fault systems in sandbox experiments. Paper 1: 2D hanging wall deformation and section restoration. Journal of Structural Geology 25, 1551–1560.